AD-A186 236 HIGHER HARMONIC GENERATION IN THE INDUCED RESONANCE ELECTRON CYCLOTRON MA..(U) SCIENCE APPLICATIONS INTERNATIONAL CORP MCLEAN VA S RIYOPOULOS ET AL. 1/1

UNCLASSIFIED SEP 87 NRL-MR-6072 DE-AI05-83ER40117 F/G 9/3 NL

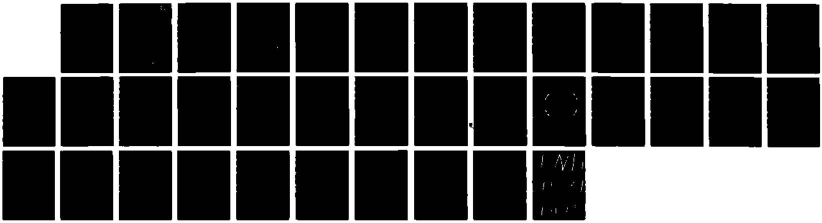

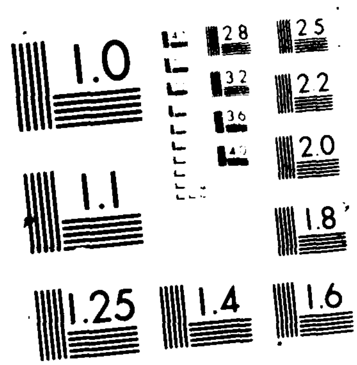
1.0
2.8
2.5
3.2
2.2
3.6
2.0
1.1
1.8
1.25
1.4
1.6

aval Research Laboratory
shington, DC 20375-5000

(2)

NRL Memorandum Report 6072

Higher Harmonic Generation in the Induced Resonance Electron Cyclotron Maser

S. RIYOPOULOS,* C. M. TANG, P. SPRANGLE AND B. LEVUSH†

Plasma Theory Branch
Plasma Physics Division

**Science Applications International Corp.*
McLean, VA 22102

†University of Maryland
College Park, MD 20742

September 24, 1987

SECURITY CLASSIFICATION OF THIS PAGE

REPORT DOCUMENTATION PAGE

1a. REPORT SECURITY CLASSIFICATION UNCLASSIFIED	1b RESTRICTIVE MARKINGS
2a. SECURITY CLASSIFICATION AUTHORITY	3 DISTRIBUTION / AVAILABILITY OF REPORT Approved for public release; distribution unlimited.
2b. DECLASSIFICATION / DOWNGRADING SCHEDULE	
4. PERFORMING ORGANIZATION REPORT NUMBER(S) NRL Memorandum Report 6072	5. MONITORING ORGANIZATION REPORT NUMBER(S)
6a. NAME OF PERFORMING ORGANIZATION Naval Research Laboratory; 6b. OFFICE SYMBOL (If applicable) Code 4790	7a. NAME OF MONITORING ORGANIZATION
6c. ADDRESS (City, State, and ZIP Code) Washington, DC 20375-5000	7b. ADDRESS (City, State, and ZIP Code)
8a. NAME OF FUNDING / SPONSORING ORGANIZATION U.S. Dept. of Energy; 8b. OFFICE SYMBOL (If applicable)	9. PROCUREMENT INSTRUMENT IDENTIFICATION NUMBER J.O. #47-2005-0-6
8c. ADDRESS (City, State, and ZIP Code) Washington, DC 20545	10. SOURCE OF FUNDING NUMBERS PROGRAM ELEMENT NO. DOE; PROJECT NO AI05-83 ER40117; TASK NO ORD (326); WORK UNIT ACCESSION NO. 380-537

11. TITLE (Include Security Classification)

Higher Harmonic Generation in the Induced Resonance Electron Cyclotron Maser

12. PERSONAL AUTHOR(S) Riyopoulos,[1] S., Tang, C.M., Sprangle, P., and Levush,[2] B.

13a. TYPE OF REPORT	13b. TIME COVERED	14. DATE OF REPORT (Year, Month, Day)	15. PAGE COUNT
Interim	FROM ____ TO ____	1987 September	36

16. SUPPLEMENTARY NOTATION
[1]Science Applications Intl. Corp., McLean, VA 22102
[2]University of Maryland, College Park, MD 20742

17. COSATI CODES			18. SUBJECT TERMS (Continue on reverse if necessary and identify by block number)
FIELD	GROUP	SUB-GROUP	Masers; Millimeter wavelengths; Gyrotrons; Wave particle interaction; Radiation sources

19. ABSTRACT (Continue on reverse if necessary and identify by block number)

The operation of the induced resonance electron cyclotron (IREC) maser at Doppler upshifted cyclotron harmonics is studied. A set of fast-time averaged nonlinear equations of motion is derived for the particle motion near an arbitrary harmonic at any index of refraction. The small signal efficiency is computed analytically and the minimum current to start the cavity oscillations is obtained. The nonlinear equations of motion are integrated numerically. The interaction efficiency at the first few harmonics is found comparable to the efficiency at the fundamental. The sensitivity of the efficiency to the beam thermal spreads is minimized by the proper selection of the index of refraction.

20 DISTRIBUTION / AVAILABILITY OF ABSTRACT ☒ UNCLASSIFIED/UNLIMITED ☐ SAME AS RPT ☐ DTIC USERS	21 ABSTRACT SECURITY CLASSIFICATION UNCLASSIFIED
22a NAME OF RESPONSIBLE INDIVIDUAL C. M. Tang	22b TELEPHONE (Include Area Code) (202) 767-4148; 22c. OFFICE SYMBOL Code 4791

DD FORM 1473, 84 MAR — 83 APR edition may be used until exhausted. All other editions are obsolete

SECURITY CLASSIFICATION OF THIS PAGE

CONTENTS

HIGHER HARMONIC GENERATION IN THE INDUCED RESONANCE ELECTRON CYCLOTRON MASER

I. INTRODUCTION

Generation of intense radiation in the microwave regime through electron cyclotron interaction was proposed independently by a number of researchers[1-4] in the late 1950s. Electrons gyrating in resonance with the radiation field experience a bunching in the relative wave particle phase through the dependence of the cyclotron frequency on the relativistic mass. High amplification of the radiation field, known as masing action, results for radiation frequencies slightly above the electron cyclotron frequency. Electron cyclotron masers[5-18], also called gyrotrons, have demonstrated efficient high power generation capability at the centimeter wavelengths. Electron cyclotron instabilities also occur in ionospheric and astrophysic plasmas[19,20].

A variety of potential applications, such as advanced accelerators, heating of fusion plasmas, short wavelength radar and spectroscopy, call for generation of intense radiation at even shorter wavelengths in the millimeter and submillimeter range. In a closed resonator, the shortest wavelength for single mode operation is tied to the transverse dimension of the cavity. Operation at radiation wavelengths shorter than the transverse dimensions will result in a multimode excitation[21] due to the small frequency separation among cavity eigenmodes. This limitation in the wavelength is considerably relaxed in the quasi-optical maser[22,23] operating in an open resonator that offers much improved frequency separation.

Considerable attention has been given lately to the operation at Doppler upshifted frequencies[24-30] resulting from a finite wave number k_z in the direction of the electron beam propagation. The operation frequency ω, defined by the resonance condition $\omega - k_z z - \Omega_c = 0$, is given by

Manuscript approved July 9, 1987.

$$\omega = \Omega_c(1 - n_z\beta_z)^{-1} ,$$

where γ is the relativistic factor $\gamma = (1-\beta^2)^{-1/2}$, $\beta = v/c$, $n_z = k_z c/\omega$ is the parallel index of refraction and $\Omega_c = \Omega_0/\gamma$ is the relativistic cyclotron frequency with $\Omega_0 = eB_0/mc$. For $n_z = \beta_z = 1$ the frequency is boosted to $2\gamma_z^2$ times the electron cyclotron frequency with $\gamma_z = (1-\beta_z{}^2)^{-1/2}$. Note that both parallel and perpendicular kinetic energy of the electrons feed the instability in case of a tilted resonator. So far plane wave configurations in simple geometry, also referred to as the cyclotron autoresonance maser[24] (CARM), have been analyzed[24-27] in conjunction with Doppler upshifting of the radiation frequency.

The induced resonance electron cyclotron (IREC) maser[28-31], shown in Fig. 1, operates at Doppler upshifted frequencies, utilizing at the same time the advantages of the open resonators. Each resonator forms an angle α with the direction of the electron beam along the external magnetic field. The index of refraction $n_z = \cos\alpha$ is adjustable by varying the angle between the resonators and can be chosen to minimize the effects of finite beam thermal spreads. For operation at the optimum refraction index the efficiency is relatively insensitive to the beam energy spread. The sensitivity to the beam pitch angle spread can also be minimized. The interaction length inside the resonator that maximizes efficiency is of the order of half a bounce distance[14] for the trapped particles.

As the available magnetic field limits the maximum operation frequency for given γ, operation at higher harmonics[31,32] becomes very attractive. The magnetic field required to produce radiation at a given frequency is reduced to a fraction $1/(N + 1)$ for operation at the Nth harmonic. Operation at higher harmonics has been analyzed for the conventional[33,34] and quasioptical[35,36] gyrotron, showing that considerable efficiency can be achieved at the first few harmonics. Previous IREC studies have considered operation at the fundamental frequency and small Larmor radius, relevant to the case of small resonator angle and small pitch angle $\theta = v_\perp/v_z$. In the present work we analyze operation at any given harmonic N and arbitrary resonator angle including finite Larmor radius effects. The effects of the Gaussian radiation profile are retained as well. A set of slow time scale equations of motion is derived by averaging over the cyclotron period time scale. The small signal efficiency is determined analytically. Nonlinear efficiency is determined by numerical integration. It is found that the efficiency for the first few harmonics is comparable to that for the fundamental in the same parameter regime. This is feasible because saturation occurs at larger radiation amplitude with higher harmonics. The effects of energy, pitch angle and guiding center spread are also studied. An optimum resonator angle α exists for a given set of parameters minimizing the effects of finite beam thermal spreads. Efficiency enhancement can be achieved by properly tapering the external magnetic field[29], inducing an extended wave particle resonance.

The remainder of this paper is organized as follows. In Section II, we describe the field in the resonator and we obtain the fast-time averaged equation of motion. In Section III, the small signal efficiency and the start-up current required to trigger the oscillations in the resonator are calculated. In Section IV, we discuss briefly the effects caused by the finite thermal spreads in the electron energy and pitch angle. In Section V, we integrate numerically the equations of motion using velocity distributions with finite energy and pitch angle spread as well as guiding center distribution in the transverse direction. The nonlinear efficiency is computed for the first few harmonics.

II. FIELD MODELING AND PARTICLE DYNAMICS

The configuration for the induced resonance electron cyclotron (IREC) maser is shown schematically in Fig. 1. The interaction cavity is formed by the two quasi-optical resonators intersecting at an angle 2α where α is the angle relative to the external magnetic field B_o along the z-axis. The electron beam also propagates along z. The total vector field is the superposition of the two resonant fields

$$A(x',y',z';t)_{\alpha} + A(x',y',z';t)_{-\alpha}, \tag{1}$$

where $A(x',y',z';t)$ are eigenmodes of the Fabry-Perot type resonator. Here we consider the lowest order Gaussian TEM_{00} modes linearly polarized along the y-axis

$$A(x',y',z';t) = \hat{e}_y \frac{1}{4} A_o \exp\left[-i\left(\frac{k}{2}\frac{x'^2+y'^2}{q(z')} - \mu(z')\right)\right] \left\{\exp\left[i(kz'-\omega t)\right] + \exp\left[-i(kz' + \omega t')\right]\right\} + c.c., \tag{2}$$

where

$$\frac{1}{q(z')} = \frac{1}{R(z')} - i\,\frac{\lambda}{\pi w^2(z')}, \qquad R(z') = z'\left[1 + \left(\frac{z'}{Z_o}\right)^2\right],$$

$$w(z') = w_o\left[1 + \left(\frac{z'}{Z_o}\right)^2\right]^{1/2}, \qquad \mu(z') = \tan^{-1}\left(\frac{z}{Z_o}\right),$$

w_o is the beam waist at the center of the resonator, λ is the wavelength and $Z_o = \pi w_o^2/\lambda$ is the Rayleigh length.

The coordinates $(x',y',z')_{\pm\alpha}$ have the z'-axis aligned with each resonator and are related to (x,y,z) by

$$\begin{pmatrix} x' \\ z' \end{pmatrix} = \begin{pmatrix} \cos\alpha & \pm\sin\alpha \\ \pm\sin\alpha & \cos\alpha \end{pmatrix} \begin{pmatrix} x \\ z \end{pmatrix}, \tag{3}$$
$$y' = y,$$

The radiation field is assumed at temporarily steady state. The Gaussian width w_o for the radiation envelope is much larger than the radiation wavelength λ and the beam spot size b. The Rayleigh length Z_o is typically much longer than the interaction length $L \sim w_o/\sin\alpha$ in the z-direction. In the vicinity of the beam $x \sim y \sim b$, and within the interaction regime $|z| \sim L$, we have $b/L \sim z/Z_o \sim \varepsilon << 1$, $b/Z_o \sim \varepsilon^2$. Combining Eqs. (1) - (3), and dropping terms of order ε^2, the forward propagating component of the total field near the interaction area is expressed as

$$A_t(x,y,z;t) = \hat{e}_y A_o e^{-\frac{z^2\sin^2\alpha}{w_o^2}} \cos k_\perp x \cos (k_z z-\omega t), \tag{4}$$

where $k_\perp = (\omega/c) \sin \alpha$, $k_z = (\omega/c) \cos \alpha$.

In short, Gaussian effects in the transverse direction of order $b^2/L^2 \sim \varepsilon^2$ have been omitted while the electrons experience a Gaussian envelope of effective width $L = w_o/\sin\alpha$ in the z-direction. Only the forward propagating wave phase is considered in Eq. (4) since the synchronous interaction of an electron with the backward component occurs at down-shifted cyclotron frequency, of small practical interest.

We use the guiding center description for the particle orbits

$$\begin{aligned} x &= x_g + \rho \sin \zeta , \qquad & y &= y_g - \rho \cos \zeta, \\ p_x &= p_{gx} + p_\perp \cos \zeta , \qquad & p_y &= p_{gy} + p_\perp \sin \zeta, \end{aligned} \tag{5}$$

with (x_g,y_g) and (p_{gx},p_{gy}) denoting the guiding center position and momentum, ρ is the Larmor radius, $p_\perp$ is the magnitude of the transverse momentum and ζ is the gyroangle. By averaging the exact Lorentz force equations in the vector potential representation over the fast (cyclotron) time scale, the slow time scale nonlinear relativistic equations of motion are cast in the form

$$\frac{dx_g}{dz} = - \frac{\Delta\omega}{\Omega_o} \frac{\gamma}{u_z} a J_N(k_\perp \rho) \sin \psi_N \cos g_N, \tag{6a}$$

$$\frac{dy_g}{dz} = \frac{ck_\perp}{\Omega_o} \gamma \frac{u_\perp}{u_z} a J_N'(k_\perp \rho) \cos \psi_N \cos g_N, \tag{6b}$$

$$\frac{du_\perp}{dz} = \left(\frac{\gamma\omega}{cu_z} - k_z\right) a J_N'(k_\perp \rho) \sin \psi_N \sin g_N, \tag{6c}$$

$$\frac{du_z}{dz} = k_z \frac{u_\perp}{u_z} a J_N'(k_\perp \rho) \sin \psi_N \sin g_N, \tag{6d}$$

$$\frac{d\psi_N}{dz} = - \frac{\gamma\Delta\omega}{cu_z} + \frac{N^2}{u_\perp} \left(\frac{\gamma\omega}{cu_z} - k_z\right) a \frac{J_N'(k_\perp \rho)}{k_\perp \rho} \cos \psi_N \sin g_N$$

$$- N \frac{k_\perp}{u_z} a J_N(k_\perp \rho) \cos \psi_N \sin g_N. \tag{6e}$$

In Eqs. (6a) to (6e) the prime (′) signifies the Bessel function derivative in respect to the argument, u is the normalized momentum $u = p/mc = \gamma v/c$, γ is the relativistic factor $\gamma = (1 + u_\perp^2 + u_z^2)^{1/2}$, $\psi_N = k_z z - \omega t + N\zeta + N\pi/2$ is the relative phase between the field and the particle, $g_N = k_\perp x_g - N\pi/2$ carries the dependence on the guiding center position, $a(z) = a_o \exp(-z^2/L^2)$ is the normalized radiation amplitude with $a_o = eA_o/mc^2$ and the detuning in frequency $\Delta\omega$ is given by

$$\Delta\omega = \omega(1-n_z\beta_z) - N\Omega_o/\gamma. \tag{7}$$

It is the dependence of the detuning $\Delta\omega$ on the particle energy through the relativistic correction γ that causes the phase bunching and the radiation amplification in the linear regime. The evolution of γ is found combining Eqs. (6c) to (6e),

$$\frac{d\gamma}{dz} = \frac{\omega}{c} \frac{u_\perp}{u_z} a\, J_N'(k_\perp \rho) \sin \psi_N \sin g_N. \tag{8}$$

In performing the fast time averaging to obtain Eqs. (6)-(8) we have assumed that the particles always remain close to resonance with a single harmonic N, i.e., $\omega(1-n_z\beta_z) - N\Omega_o/\gamma \simeq 0$. Therefore the change in energy $\Delta\gamma$ and consequently the radiation amplitude a_o cannot exceed a certain limit. When a_o is very large, the particles may also experience resonant effects from nearby harmonics $N \pm 1$. The validity conditions for a single resonant harmonic are satisfied in the parameter regime under consideration.

The nonlinear system of differential equations (6)-(8) cannot be solved analytically in terms of elementary functions, except in some special cases[37,38]. We resort to numerical integration in order to examine the nonlinear behavior while the small signal analysis is done by perturbation theory.

III. SMALL SIGNAL EFFICIENCY

One of the issues concerning intense microwave generation is the intrinsic efficiency η of the interaction, defined as

$$\eta = -\frac{\langle\gamma_f-\gamma_o\rangle}{\langle\gamma_o-1\rangle} = -\langle\gamma_o-1\rangle^{-1}\int dp_o^3 f(p_o)\int dg_o\int d\psi_o\int_{-\infty}^{\infty} dz\,\frac{d\gamma}{dz}, \tag{9}$$

where < > signifies the average over the initial distribution in phase space, and γ is a function of the initial conditions $\gamma(z;\, p_{\perp o},\, p_{zo},\, \psi_o,\, g_o)$ with $\psi_o = \psi_N(-\infty)$ and $g_o = g_N(-\infty)$. We compute the small signal efficiency in order to determine the beam current required to overcome losses and start the cavity oscillations. After obtaining the linearized solutions of Eqs. (6) to (8), we substitute them into the integrant in the right-hand side of Eq. (9). The evaluation of the final result is considerably simplified by taking the phase space average over ψ_o before the spatial integration[22,36] over z. Expanding the products of trigonometric terms inside the integrant into sums, averaging over ψ_o and extending the limits of the z-integration to $\pm\infty$, we obtain the linear efficiency in terms of the initial conditions

$$\eta = \frac{\pi}{4}\,\frac{a_o^2\,\xi^2}{\gamma_o(\gamma_o-1)}\left(J_N'(s_o)\right)^2 \exp\left(-\frac{1}{2}\,\xi^2\,\frac{\Delta\omega_o^2}{\omega^2}\right)\langle\sin^2 g_o\rangle$$

$$\left\{\left(n_z\beta_{zo}-1\right)\left(1+\frac{N^2 J_N(s_o)}{s_o J_N'(s_o)}+\frac{s_o J_N''(s_o)}{J_N'(s_o)}\right)+\theta_o\beta_{zo}\left(\theta_o n_z+\frac{N J_N(s_o)}{J_N'(s_o)}\,n_\perp\right)\right.$$

$$\left.+\left(\xi^2\beta_{\perp o}^2(1-n_z^2)-\frac{\langle\cos^2 g_o\rangle}{\langle\sin^2 g_o\rangle}\,\frac{s_o J_N(s_o)}{J_N'(s_o)}\right)\left(\frac{\Delta\omega_o}{\omega}\right)-n_z\beta_{zo}\theta_o^2\xi^2\left(\frac{\Delta\omega_o}{\omega}\right)^2\right\}, \tag{10}$$

where $s_o = k_\perp\rho_o$, $g_o = k_\perp x_{go} - N\pi/2$, $\beta_{\perp o} = v_{\perp o}/c$, $\beta_{zo} = v_{zo}/c$, $\theta_o = v_{\perp o}/v_{zo}$ and $\langle f\rangle = (1/2\pi)\int_0^{2\pi} d(k_\perp x_g) f$ is the average over the initial guiding center position.

We have chosen to express η in terms of the parameters $\Delta\omega_o/\omega$ and $\xi = \omega\tau$, where $\tau = \gamma_o L/cu_{zo}$ is the transit time through the interaction regime. The argument $\xi\Delta\omega_o/\omega$ in the exponential is equal to $\Delta\omega_o\tau$, the linear advance in the relative phase $\Delta\psi_o$ over the interaction regime. The sign is determined by the angular bracket on the right-hand side of Eq. (10). Treating the bracket as a quadratic form in $\Delta\omega_o/\omega$ and keeping the lowest order contribution in $k_\perp\rho$, we find that the regime for positive efficiency is given approximately by

$$\frac{\left[(N+1)\left(1 - n_z\beta_{zo}\right) - \theta_o^2 n_z\beta_{zo}\right]}{\left(1 - n_z^2\right)\beta_{\perp o}^2\xi_o^2} < \frac{\Delta\omega_o}{\omega} < \frac{\beta_{\perp o}^2(1 - n_z^2)}{n_z\beta_{zo}\theta_o^2}.$$

The upper limit in $\Delta\omega_o/\omega$ is due to the finite n_z and results from the negative contribution of the quadratic term $(\Delta\omega/\omega)^2$ that overtakes the positive contribution of the linear terms for small angle,

$$\sin^2\alpha < \frac{n_z\beta_{zo}\theta_o^2}{\beta_{\perp o}^2}\,\frac{\Delta\omega_o}{\omega}.$$

For typical operation parameters we have $\xi \gg 1$ and $\Delta\omega_o/\omega \ll 1$. In order to estimate the maximum efficiency within the positive regime, we parametrize Eq. (10) as a function of $\zeta = \xi\Delta\omega_o/\omega$ and look for the zeros of the cubic equation resulting from $d\eta/d\zeta = 0$. If the angle α is not too small, $\sin^2\alpha \gg 1/\xi\beta_{\perp o}^2$ where $\xi \gg 1$, then the maximum occurs at $\zeta = 1$, yielding

$$\eta_{max} \simeq \frac{\pi}{8}\,\frac{a_o^2\,\xi_o^3\left(J_N'(k_\perp\rho_o)\right)^2\beta_{\perp o}^2}{(\gamma_o-1)\,\gamma_o\sin\alpha}\exp\left(-\tfrac{1}{2}\right), \qquad (12)$$

where $\xi_o^2 = \xi^2(1 - n_z^2) = (w_o\gamma_o\omega/cu_{zo})^2$ is independent of α. The small signal efficiency increases with decreasing angle α (increasing index of refraction n_z) provided that $\sin\alpha$ satisfies the inequality above Eq. (12). When $\sin\alpha$ is too small, an exact solution of the cubic equation for ζ is required and Eq. (12) is invalid.

We now calculate the start-up beam current using the small signal efficiency. Amplification of the electromagnetic radiation is possible if

$$\eta P_b > \frac{dE}{dt} = \frac{\omega}{Q} E, \tag{13}$$

where $E = (1/4)w_o^2 \, L_R a_o^2(\omega^2/c^2)(m^2c^4/|e|^2)$ is the total energy stored inside both resonators, L_R is the resonator length, dE/dt is the combined refraction, diffraction and transmission losses and Q is the quality factor for the cavity. Combining Eqs. (12) and (13) we obtain

$$I_s V_b > 2 \, \frac{\beta_{zo}^3}{\beta_{\perp o}^2} \, \frac{\gamma_o(\gamma_o - 1) \sin\alpha \exp(-\frac{1}{2})}{\pi[J_N'(k_\perp \rho_o)]^2} \, \frac{m^2c^5}{|e|^2} \, \frac{L_R}{w_o Q}. \tag{14}$$

For small Larmor radius $k_\perp \rho_o << 1$ the start-up current I_s increases very quickly with the harmonic N, $I_s \propto 2^{2N}[(N-1)!]^2/(k_\perp \rho_o)^{-(N-1)}$. It is therefore desirable to operate at $k_\perp \rho_o \geq 1$ in order to have good coupling to the resonator modes and low start-up currents. In this case the start-up current scales roughly as the inverse maximum of the Bessel function derivative, $I_s \propto N^{1/3}$, increasing mildly with the harmonic N. We can achieve harmonic selection by choosing $k_\perp \rho_o$ near a maximum of $J_N'(k_\perp \rho_o)$ for the intended Nth harmonic.

Expression (14) for the start-up current was derived using coherent resonator modes. These modes have evolved from an initial noise background of spontaneous cyclotron radiation. During the spontaneous emission stage preceding coherency most of the emitted radiation is contained within a cone of angle $1/\gamma$ around the direction of the particle velocity v. Since v makes an angle $\Theta = \tan(v_\perp/v_z)$ with the magnetic field the condition $|\Theta - \alpha| \leq 1/\gamma$ must be met to avoid excessive losses during the start-up phase.

IV. THERMAL EFFECTS

One of the important features associated with the IREC maser is choosing the index of refraction appropriately to minimize the effects of the electron beam thermal spreads. Spreads in the initial electron momentum will cause a spread in the detuning parameters $\Delta\omega_o$ among different particles. This in turn will cause an accelerated mixing in phase space opposing the nonlinear phase bunching and reducing in efficiency. According to Eq. (7) a standard deviation

$$\delta(\Delta\omega)_o = \left[\left(\frac{\partial\Delta\omega}{\partial\beta}\right)^2 \delta\beta_z^2 + \left(\frac{\partial\Delta\omega}{\partial\beta_\perp}\right)^2 \delta\beta_\perp^2\right]^{1/2} = \left[(\omega n_z - N\Omega_o\gamma_o\beta_{zo})^2\delta\beta_z^2 + (N\Omega_o\gamma_o\beta_{\perp o})^2\delta\beta_\perp^2\right]^{1/2} \tag{15}$$

in the initial detuning results from a beam distribution with velocity deviations $\delta\beta_z$ and $\delta\beta_\perp$. The choice of resonator angle

$$n_z = \cos\alpha = \frac{N\Omega_o\gamma_o\beta_{zo}}{\omega} \tag{16}$$

causes the minimum initial spread in $\Delta\omega_o$ for any beam thermal spreads. The minimum spread from Eqs. (15) and (16) can also be expressed in terms of the pitch angle spread $\delta\theta_o$ and the energy spread $\delta\gamma_o$. Then, the requirement for small phase mixing among various particles over the interaction length L, namely $\delta(\Delta\omega)_o L/c\beta_z \ll \pi$, suggests

$$\frac{\delta\theta_o}{\theta_o} + \frac{1}{\gamma_o^2}\frac{\delta\gamma_o}{\gamma_o} \ll \frac{\beta_{zo}}{2N_c(N\beta_{\perp o}^2\gamma_o^2)}, \tag{17}$$

where $N_c = \Omega_o L/(2\pi\gamma_o c\beta_{zo})$ is the approximate number of cyclotron gyrations within the interaction length. The beam thermal spread requirements become more stringent with increasing harmonic N.

In the nonlinear operation regime the electrons get trapped in the wave potential[14,38] and execute synchrotron oscillations in phase space in a similar manner as in the conventional gyrotrons. The phase mixing among various particles is now determined by the dependence of the trapped particle synchrotron period on the various parameters. The efficiency deterioration involves more factors than the initial spread in the detuning $\Delta\omega_0$, which is the dominant source of phase mixing only in the small signal regime $a_0 << 1$. Analytic predictions similar to Eq. (16) are hard to make in the nonlinear case. Our numerical results show that when the index of refraction is optimized according to (16) the nonlinear efficiency is practically insensitive to the energy spread $\delta\gamma_0/\gamma_0$.

V. NUMERICAL RESULTS

In this section, we investigate various aspects of the nonlinear performance by numerically integrating Eqs. (6a) to (6e). We consider an electron beam of $\gamma_o = 2.5$ (~ 0.75 MeV) with $\beta_{\perp o} = 1/\gamma_o$ and $\beta_{zo} = 0.825$ in a guide magnetic field of strength $B_o = 40$ kG. The appropriate index of refraction to minimize the effect of energy spread is, according to Eq. (16), $n = 0.982$ which corresponds to an angle $\alpha = 11°$. The frequency is upshifted by a factor $N/(1 - n\beta_{zo}) = 5.26$ N times the relativistic cyclotron frequency, and corresponds to a wavelength of 0.41 mm for the third harmonic $N = 3$ and 0.31 mm for the fourth harmonic $N = 4$. The radiation spot size w_o is 0.50 cm and the Rayleigh lengths are 14.3 cm and 25.8 cm for $N = 3$ and $N = 4$ respectively. We consider a uniform guiding center distribution in the interval $0 < k_{\perp}x_g < 2\pi$.

Curves of efficiency η versus a_o for various values of the detuning $\Delta\omega_o/\omega$ are plotted for $N = 3$ and $N = 4$ in Figs. 2 and 3 respectively. These results correspond to a cold beam without thermal spreads. We find the efficiency for the first few harmonic comparable to the efficiency for the fundamental[29] under the same operation parameters. Efficiency saturation occurs for larger amplitude a_o compared to the operation at the fundamental. Figure 4 shows the effects of finite beam quality on efficiency when the electron beam has either a spread in the pitch angle or a spread in energy. We plot the ratio of the thermalized efficiency η over the cold beam efficiency η_o for the third harmonic $N = 3$ at fixed amplitude $a_o = 0.20$. Curve (a) for zero energy spread, $\Delta\gamma_o/\gamma_o = 0$, shows that the half width in the pitch angle spread that reduces efficiency by 50%, is equal to $\Delta\theta_o/\theta_o = 2\%$. Curve (b) for zero pitch angle spread, $\Delta\theta_o/\theta_o = 0$, shows that the half width in energy spread is $\Delta\gamma_o/\gamma_o = 13\%$. Efficiency tends to be more sensitive on the spread in the pitch angle than the spread in energies; therefore, we may simulate thermal effects by including only pitch angle spreads, cutting down on computing time.

Given that the large signal efficiency depends on few parameters, predictions about optimum operation at maximum efficiency are hard to make. One anticipates maximum efficiency when the transit time through the interaction regime is about equal to half the synchrotron period for a trapped particle. An optimum interaction length in the z direction $L_z = 2L = 2w_o/\sin\alpha$ corresponds to a given synchrotron period ω_b, which, in turn, depends on the five parameters a_o, γ_o, θ_o, $\Delta\omega_o$ and $\cos\alpha$. This is illustrated in Fig. 5, which shows efficiency as a function of the traveled distance z for three different Gaussian profiles corresponding to different radiation spot sizes w_o, keeping the other parameters fixed. In curve (a) the interaction length is less than half the bounce distance $L_b = \pi c \beta_z/\omega_b$ and the electrons exit the resonator before reaching the point of lowest energy in their trajectories. In curve (b) we have a good matching of L_z with L_b achieving the highest efficiency. In curve (c) L_z is larger than L_b and the electrons overshoot the point of minimum energy, gaining energy back from the wave and reducing effic·ency.

From the practical point of view, one would like to optimize the design parameters of the resonator α and L for a given beam energy γ_o and pitch angle θ_o under the maximum energy load a_o^2 sustained by the cavity. We already picked the operation angle $\cos\alpha$ so as to minimize the effects the beam energy spread. In Fig. 6 we show the efficiency as a function of the interaction length L_z by varying the spot size w_o and keeping all other parameters fixed. The upper curve shows the nonlinear efficiency for a monoenergetic electron beam of infinitesimal spot size $b \ll w_o$, and a uniform spread in the initial phase $0 \leq \psi_o \leq 2\pi$. A uniform guiding center distribution $0 \leq k_\perp x_g \leq 2\pi$ is included in the second curve. The resulting efficiency reduction is no more than 30% indicating that some bunching in the guiding center position takes place as well. The addition of a 2% energy spread $\delta\gamma_o/\gamma_o$ with zero pitch angle spread does not reduce efficiency considerably in the fourth curve. A 2% spread in the pitch angle $\delta\theta_o/\theta_o$ with zero energy spread has a more pronounced effect on efficiency shown in the lowest curve (d). The overall picture shows that, for the parameters chosen, efficiency has a weak dependence on the interaction length L falling off slowly after an optimum length of L ~ 4 cm.

ACKNOWLEDGMENT

This work was supported by the Department of Energy under Contract DE-AI05-83ER40117, Modification 3.

REFERENCES

1. R. Q. Twiss, Aust. J. Phys. 11, 564 (1958).

2. A. V. Gaponov, Isv. Vyssh. Uchebn, Zaved, Radiofiz., 2, 450 (1959).

3. R. H. Pantell, Proc. IRE, 47, 1146 (1959).

4. J. Schneider, Phys. Rev. Lett. 2, 504 (1959).

5. J. L. Hirshfield and J. M. Wachtel, Phys. Rev. Lett. 12, 533 (1964).

6. A. V. Gaponov, M. I. Petelin and V. K. Yulpalov, Radio Phys. Quantum Electron. 10, 794 (1967).

7. V. L. Bratman, M. A. Moiseev, M. I. Petelin and R. E. Erm, Radio Phys. Quantum Electron. 16, 474 (1973).

8. D. V. Kisel, G. S. Korablev, V. G. Navel'yev, M. I. Petelin and Sh. E. Tsimring, Radio Eng. Electron. Phys. 19, No. 4, 95 (1974).

9. N. I. Zaytsev, T. B. Pankratova, M. I. Petelin and V. A. Flyagin, Radio Eng. Electron. Phys. 19, No. 5, 103 (1974).

10. V. L. Granatstein, M. Herndon, R. K. Parker and P. Sprangle, IEEE J. Quantum Electron. QE-10 No. 9, p. 651 (1974).

11. E. Ott and W. M. Manheimer, IEEE Trans. Plasma Science PS-3, 1 (1975).

12. V. L. Granatstein, P. Sprangle, M. Herndon and R. K. Parker, J. Appl. Phys. 46, 2021 (1975).

13. P. Sprangle and W. M. Manheimer, Phys. Fluids 18, 224 (1975).

14. P. Sprangle and A. T. Drobot, IEEE Trans. Microwave Theory and Techniques MTT-25, 528 (1977).

15. J. L. Hirshfield and V. L. Granatstein, IEEE Trans. Microwave Theory and Tech. MTT-25, 522 (1977).

16. K. R. Chu and J. L. Hirshfield, Phys. Fluids 21, 461 (1978).

17. V. L. Bratman, N. S. Ginzburg and M. I. Petelin, Optics Commun. 30, 409 (1979).

18. P. Sprangle and R. A. Smith, J. Appl. Phys. 51, 6, p. 3001 (1980).

19. C. S. Wu and L. C. Lee, Astrophys. J. 230, 621 (1979).

20. P. L. Pritchett, Phys. Fluids 29, 2919 (1986).

21. A. Bondeson, W. M. Manheimer and E. Ott, Infrared and Millimeter Waves 9, 309 (1983).

22. P. Sprangle, J. L. Vomvorides and W. M. Manheimer, Appl. Phys. Lett. 38, 310 (1981); also Phys. Rev. A23, 3127 (1981).

23. J. L. Vomvorides and P. Sprangle, Phys. Rev. A25, 931 (1982).

24. M. I. Petelin, Radiophysics and Quant. Electron. 17, 686 (1974); also V. L. Bratman, N. S. Ginzburg and M. I. Petelin, Optics Commun. 30, 409 (1979).

25. V. L. Bratman, G. G. Denisov, N. S. Ginzburg and M. I. Petelin, IEEE J. Quantum Electronics QE-19, 282 (1983).

26. K. E. Kreisher and R. J. Temkin, Infrared and Millimeter Waves, 7, 377 (1983).

27. A. W. Fliflet, Intl. J. Electron. 61, 1049 (1986).

28. P. Sprangle, C. M. Tang and P. Serafim, Nucl. Instr. and Methods in Phys. A250, 361 (1986).

29. P. Sprangle, C. M. Tang and P. Serafim, Appl. Phys. Lett. 49, 1154 (1986).

30. S. Riyopoulos, C. M. Tang and P. Sprangle, Phys. Rev. A36, xxxx (1987)

31. C. M. Tang, S. Riyopoulos and P. Sprangle, Proc. Eighth Intl. Conf. on Free Electron Lasers, Glasgow, Scotland, (North Holland, ed. M. Poole) pg. xxx, 1986.

32. V. L. Bratman, N. S. Ginzburg and A. S. Sergeev, Sov. Phys. JETP 55, 479 (1985).

33. A. V. Gaponov, V. A. Flyagin, A. L. Goldenberg, G. S. Nusinovich, Sh. E. Tsimring, V. G. Usov and S. N. Vlasov, Intl. J. Electron. 51, 277 (1981).

34. B. G. Danly and R. J. Temkin, Phys. Fluids 29, 561 (1985).

35. B. Levush, A. Bondeson, W. M. Manheimer and E. Ott, Intl. J. Electron. 54, 749 (1983).

36. B. Levush and W. Manheimer, IEEE Trans. of Microwave Th. and Techn. MTT-32, 1398 (1984)

37. Y. Gell, J. R. Torstensson, H. Wilhelmsson and B. Levush, Appl. Phys. B27, 15 (1982)

38. J. L. Vomvorides, Intl. J. Electron. 53, 555 (1982).

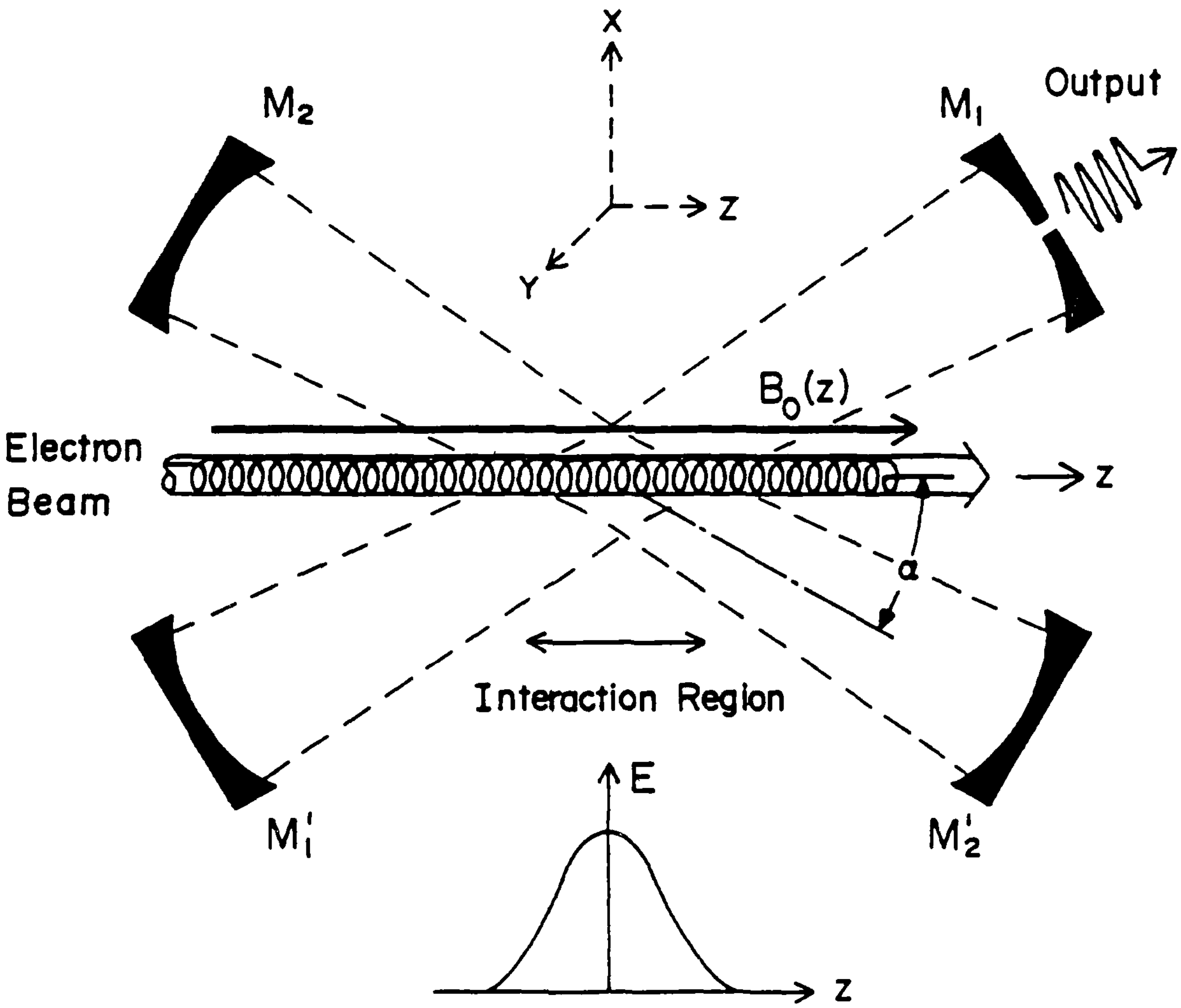

Figure 1. Schematic illustration of the Induced Resonance Electron Cyclotron Maser.

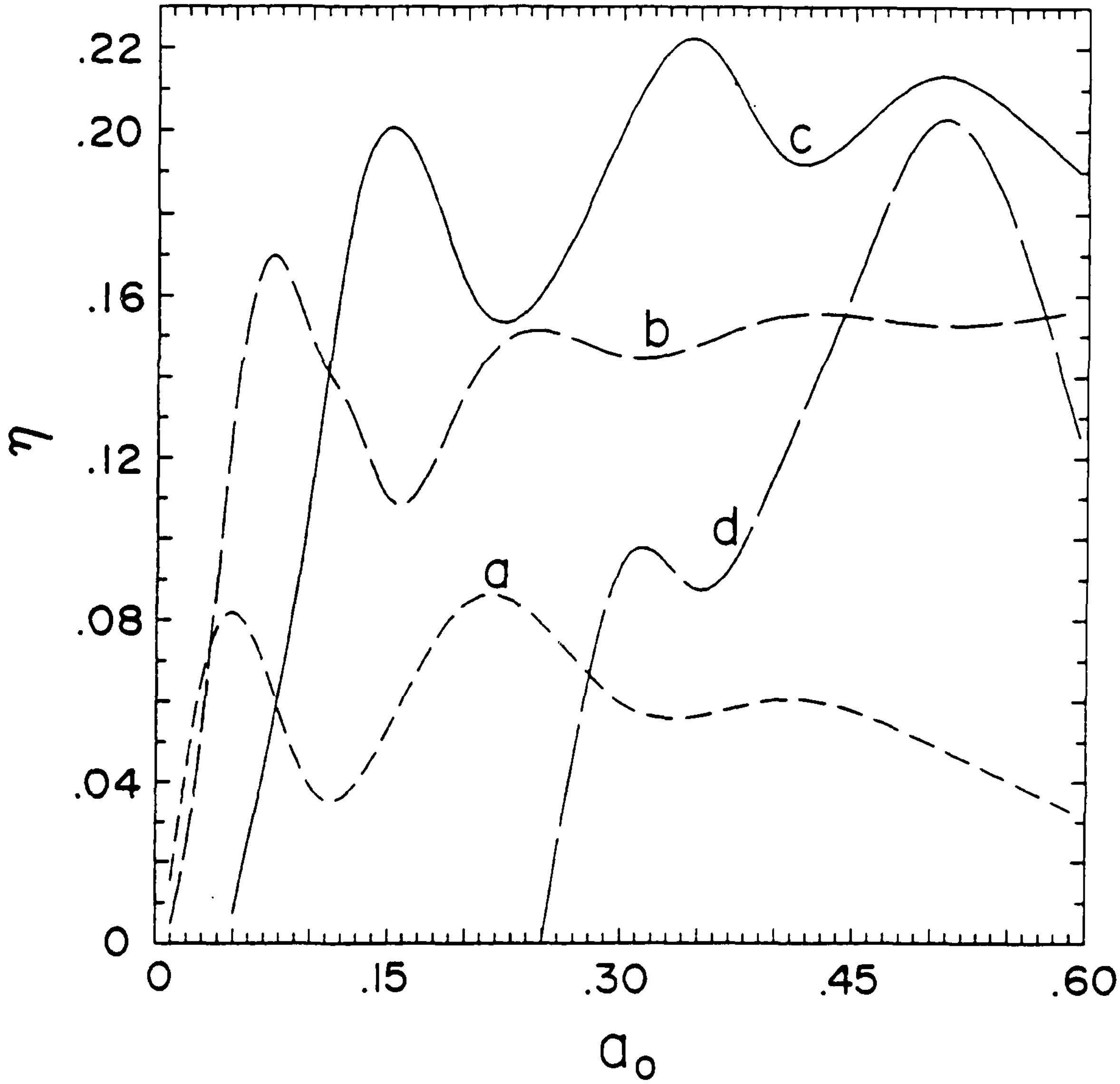

Figure 2. Plots of efficiency η versus the normalized radiation amplitude a_0 at the third harmonic N = 3 and for detuning parameters $\Delta\omega_0/\omega$ equal to (a). 0.025 (b). 0.050 (c). 0.075 and (d). 0.100 respectively. A cold beam of uniform guiding center spread is considered. The simulation parameters are $\gamma_0 = 2.5$, $\alpha = 11°$, $w_0 = 0.5$ cm and $\theta_0 = 0.48$.

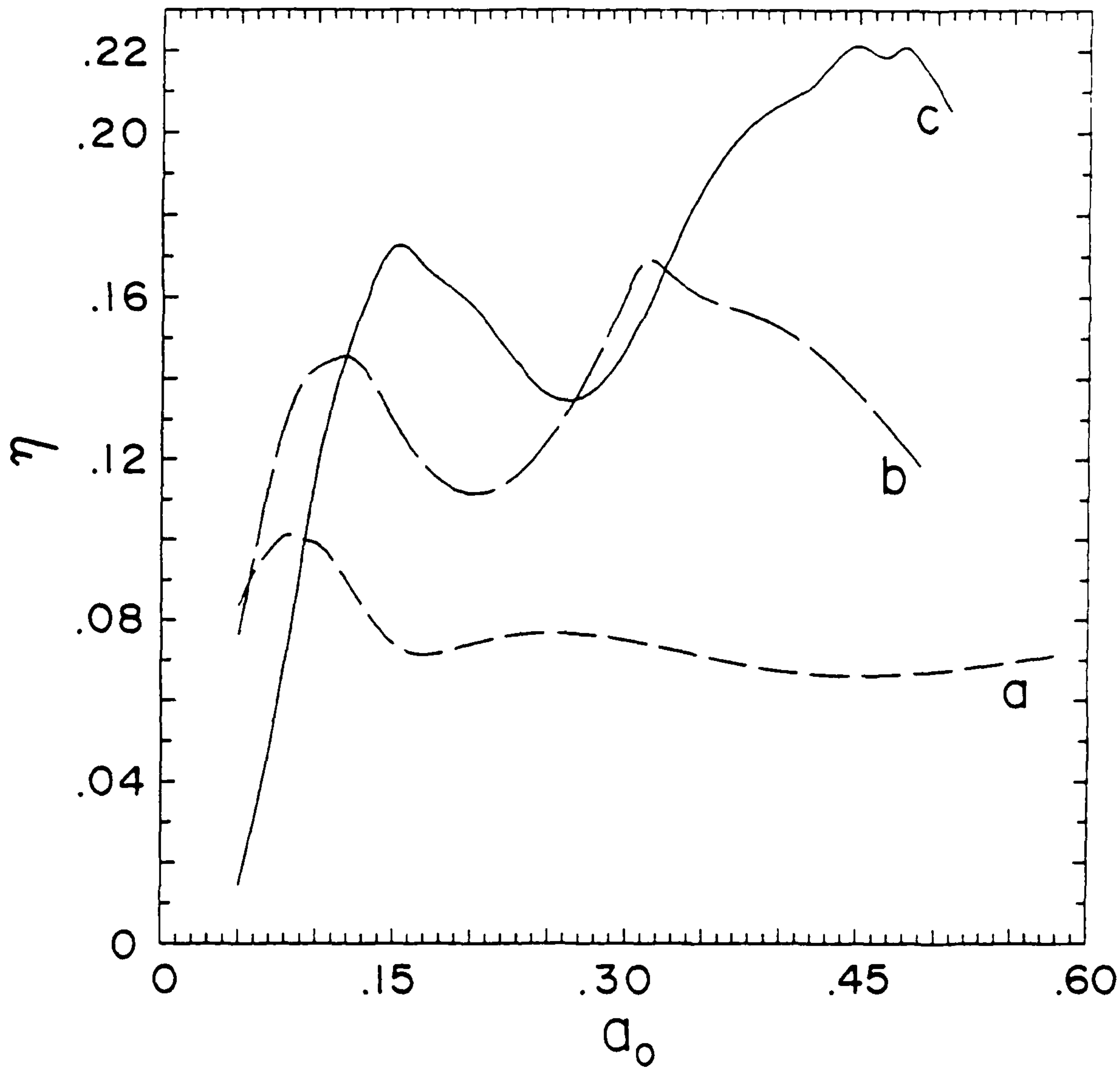

Figure 3. Plots of efficiency η versus the normalized radiation amplitude a_o at the fourth harmonic N = 4 for detuning parameter $\Delta\omega_o/\omega$ equal to (a). 0.025 (b) 0.037 and (c) 0.050 respectively. The other parameters are the same as in Fig. 2.

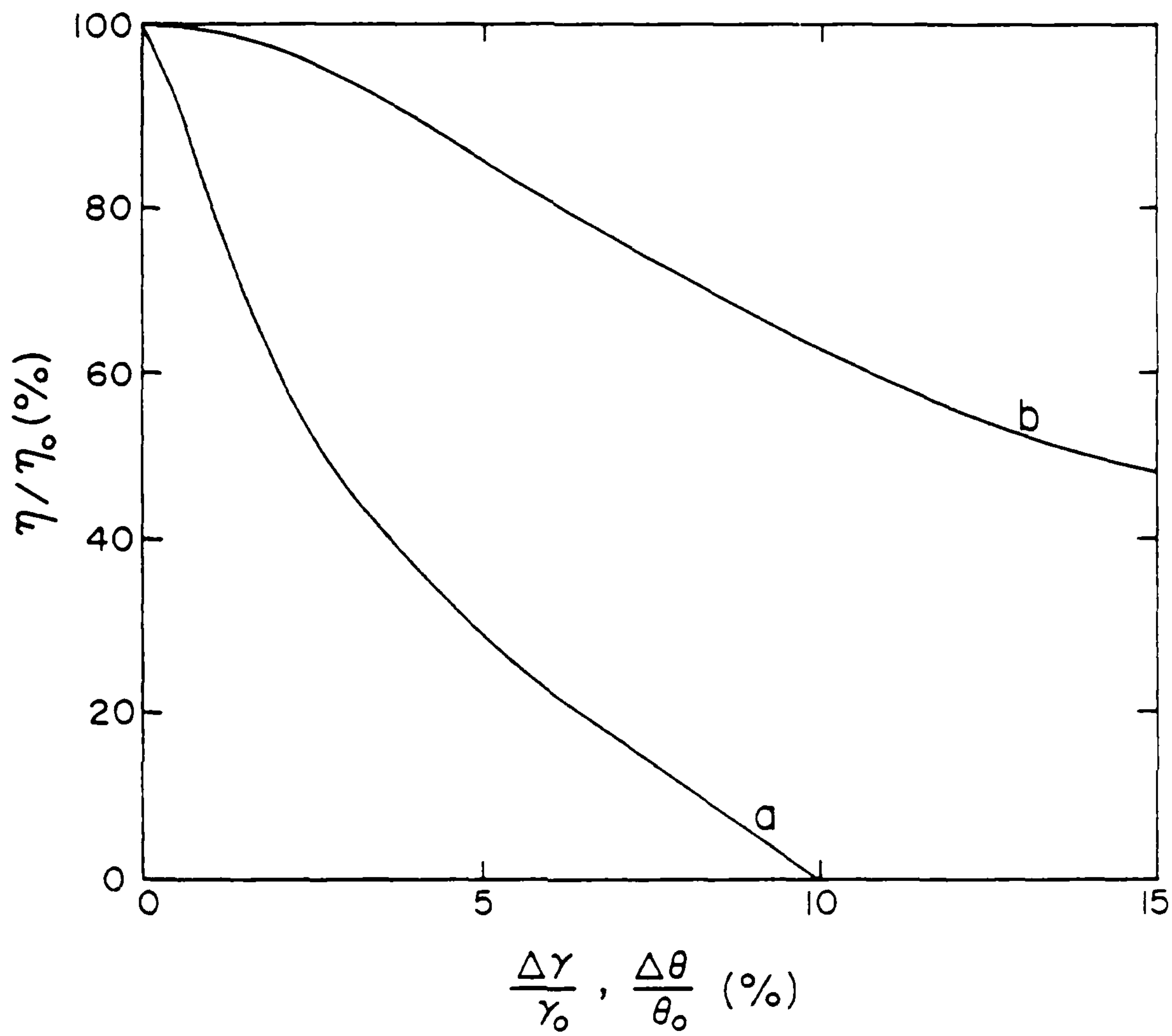

Figure 4. Dependence of the efficiency on beam thermal spreads. Shown is the ratio of thermalized to cold beam efficiency η/η_0 as a function of (a) pitch angle spread $\delta\theta_0/\theta_0$ with $\delta\gamma_0 = 0$ and (b) energy spread $\delta\gamma_0/\gamma_0$ with $\delta\theta_0 = 0$. The parameters are the same as in Fig. 2 with $\Delta\omega_0/\omega = 0.075$.

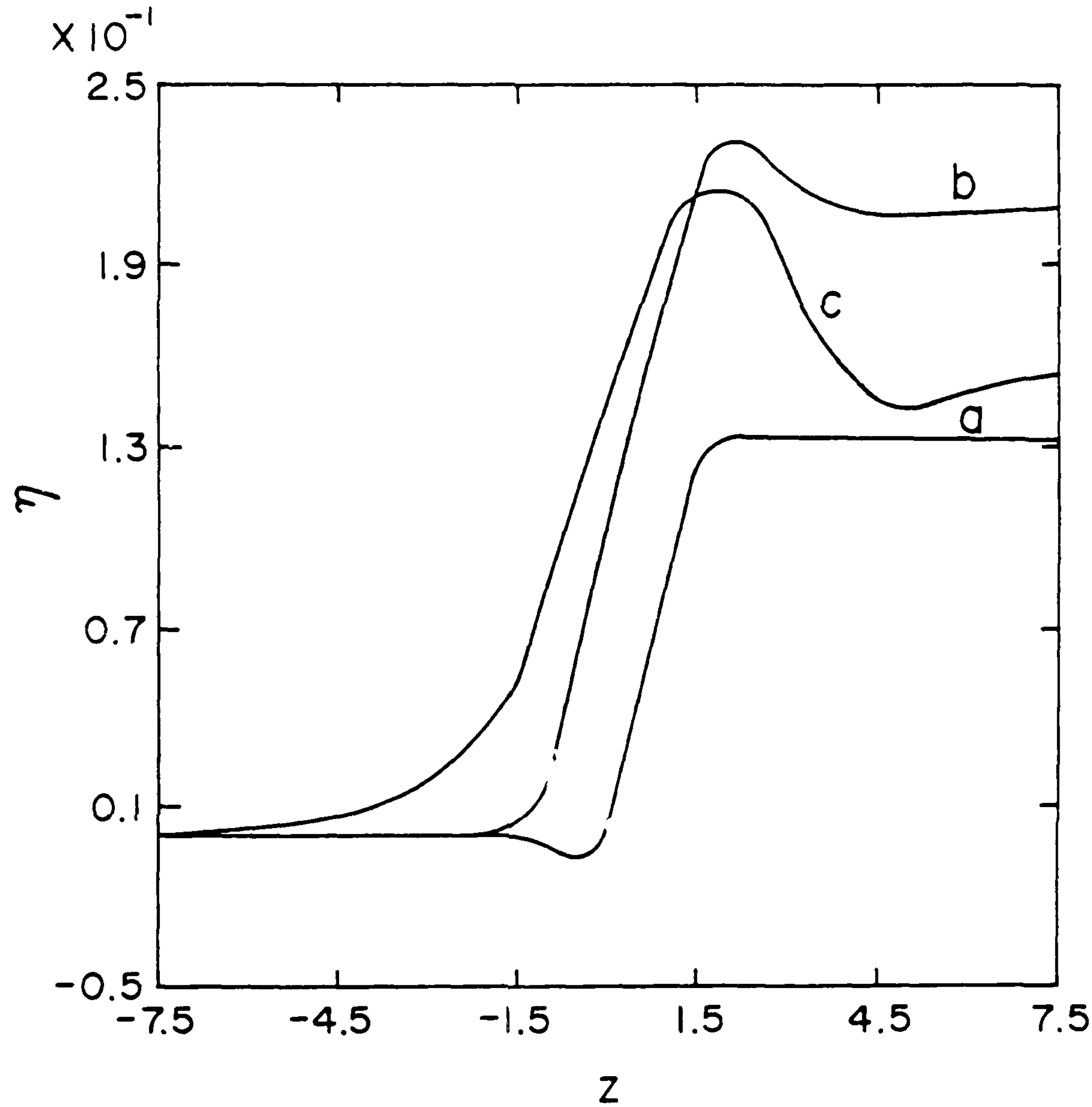

Figure 5. Plots of efficiency η versus travelled distance z inside the resonator for various interaction lengths corresponding to different radiation spot sizes w_0. The center of the resonator is at $z = 0$. L_z is equal to (a) 2.64 cm (b) 4.24 cm and (c) 7.41 cm. The parameters are the same as in Fig. 2 with $\Delta\omega_0/\omega = 0.075$.

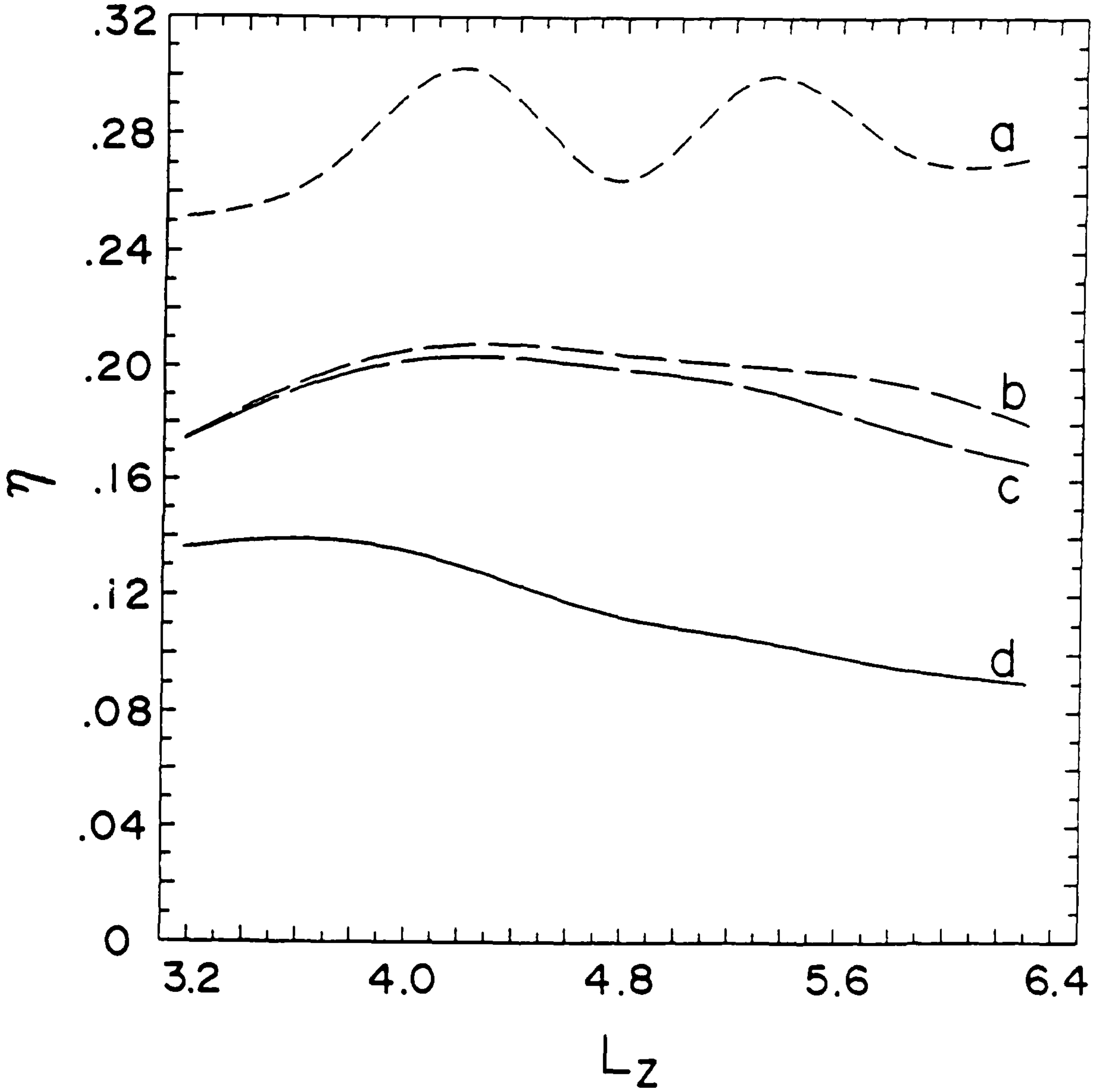

Figure 6. Plots of efficiency η versus interaction length L_z with the same parameters as before. Curve (a) is for a cold beam of zero cross section and curves (b)-(d) for a uniform guiding center spread with (b) no thermal spreads (c) 2% energy spread and (d) 2% pitch angle spread.

DISTRIBUTION LIST*

Naval Research Laboratory
4555 Overlook Avenue, S.W.
Washington, DC 20375-5000

Attn: Code 1000 - CAPT William C. Miller
1001 - Dr. T. Coffey
4603 - Dr. W.W. Zachary
4700 - Dr. S. Ossakow (26 copies)
4710 - Dr. C.A. Kapetanakos
4730 - Dr. R. Elton
4740 - Dr. W.M. Manheimer
4740 - Dr. S. Gold
4790 - Dr. P. Sprangle (100 copies)
4790 - Dr. C.M. Tang (50 copies)
4790 - Dr. M. Lampe "
4790 - Dr. Y.Y. Lau
4790A- W. Brizzi
6652 - Dr. N. Seeman
6840 - Dr. S.Y. Ahn
6840 - Dr. A. Ganguly
6840 - Dr. R.K. Parker
6850 - Dr. L.R. Whicker
6875 - Dr. R. Wagner
2628 - Documents (20 copies)
2634 - D. Wilbanks
1220 - 1 copy

* Every name listed on distribution gets one copy except for those where extra copies are noted.

Dr. R. E. Aamodt
Science Applications Intl. Corp.
1515 Walnut Street
Boulder, CO 80302

Dr. B. Amini
1763 B. H.
U. C. L. A.
Los Angeles, CA 90024

Dr. D. Bach
Los Alamos National Laboratory
P. O. Box 1663
Los Alamos, NM 87545

Dr. D. C. Barnes
Science Applications Intl. Corp.
Austin, TX 78746

Dr. L. R. Barnett
3053 Merrill Eng. Bldg.
University of Utah
Salt Lake City, UT 84112

Dr. S. H. Batha
Lab. for Laser Energetics &
Dept. of Mech. Eng.
Univ. of Rochester
Rochester, NY 14627

Dr. F. Bauer
Courant Inst. of Math. Sciences
New York University
New York, NY 10012

Dr. Peter Baum
General Research Corp.
P. O. Box 6770
Santa Barbara, CA 93160

Dr. Russ Berger
FL-10
University of Washington
Seattle, WA 98185

Dr. O. Betancourt
Courant Inst. of Math. Sciences
New York University
New York, NY 10012

Dr. B. Bezzerides
MS-E531
Los Alamos National Laboratory
P. O. Box 1663
Los Alamos, NM 87545

Dr. Irving J. Bigio
Lawrence Livermore National Laboratory
P. O. Box 808, L-626
Livermore, CA 91550

Dr. Leroy N. Blumberg
U.S. Dept. of Energy
Division of High Energy Physics
ER-224/Germantown
Wash., DC 20545

Dr. Mario Bosco
University of California, Santa Barbara
Santa Barbara, CA 93106

Dr. Howard E. Brandt
Department of the Army
Harry Diamond Laboratory
2800 Powder Mill Road
Adelphi, MD 20783

Dr. Richard J. Briggs
Lawrence Livermore National Laboratory
P. O. Box 808, L-626
Livermore, CA 91550

Dr. Bob Brooks
FL-10
University of Washington
Seattle, WA 98195

Dr. Paul J. Channell
AT-6, MS-H818
Los Alamos National Laboratory
P. O. Box 1663
Los Alamos, NM 87545

Dr. A. W. Chao
Stanford Linear Accelerator Center
Stanford University
Stanford, CA 94305

Dr. Francis F. Chen
UCLA, 7731 Boelter Hall
Electrical Engineering Dept.
Los Angeles, CA 90024

Dr. K. Wendell Chen
Center for Accel. Tech.
University of Texas
P.O. Box 19363
Arlington, TX 76019

Dr. Pisin Chen
SLAC, Bin 26
P.O. Box 4349
Stanford, CA 94305

Dr. Marvin Chodorow
Stanford University
Dept. of Applied Physics
Stanford, CA 94305

Major Bart Clare
USASDC
P. O. Box 15280
Arlington, VA 22215-0500

Dr. Christopher Clayton
UCLA, 1538 Boelter Hall
Electrical Engineering Dept.
Los Angeles, CA 90024

Dr. David Cline
Dept. of Physics
University of Wisconsin
Madison, WI 53706

Dr. Bruce I. Cohen
Lawrence Livermore National Laboratory
P. O. Box 808
Livermore, CA 94550

Dr. B. Cohn
L-630
Lawrence Livermore National Laboratory
P. O. Box 808
Livermore, CA 94550

Dr. B. Cole
Univ. of Wisconsin
Madison, WI 53706

Dr. Francis T. Cole
Fermi National Accelerator Laboratory
Physics Section
P. O. Box 500
Batavia, IL 60510

Dr. Richard Cooper
Los Alamos National Laboratory
P. O. Box 1663
Los Alamos, NM 87545

Dr. Ernest D. Courant
Brookhaven National Laboratory
Upton, NY 11973

Dr. Paul L. Csonka
Institute of Theoretical Sciences
and Department of Physics
University of Oregon
Eugene, Oregon 97403

Mr. Chris Darrow
UCLA
1-130 Knudsen Hall
Los Angeles, CA 90024

Dr. J. M. Dawson
Department of Physics
University of California, Los Angeles
Los Angeles, CA 90024

Dr. A. Dimos
NW16-225
M. I. T.
Cambridge, MA 02139

Dr. J. E. Drummond
Western Research Corporation
8616 Commerce Ave
San Diego, CA 92121

Dr. Adam Drobot
Science Applications Intl. Corp.
1710 Goodridge Dr.
Mail Stop G-8-1
McLean, VA 22102

Dr. D. F. DuBois, T-DOT
Los Alamos National Laboratory
Los Alamos, NM 87545

Dr. J. J. Ewing
Spectra Technology
2755 Northup Way
Bellevue, WA 98004

Dr. Frank S. Felber
11011 Torreyana Road
San Diego, CA 92121

Dr. Richard C. Fernow
Brookhaven National Laboratory
Upton, NY 11973

Dr. H. Figueroa
1-130 Knudsen Hall
U. C. L. A.
Los Angeles, CA 90024

Dr. Jorge Fontana
Elec. and Computer Eng. Dept.
Univ. of Calif. at Santa Barbara
Santa Barbara, CA 93106

Dr. David Forslund
Los Alamos National Laboratory
P. O. Box 1663
Los Alamos, NM 87545

Dr. John S. Fraser
Los Alamos National Laboratory
P.O. Box 1663, MS H825
Los Alamos, NM 87545

Dr. P. Garabedian
Courant Inst. of Math. Sciences
New York University
New York, NY 10012

Dr. Walter Gekelman
UCLA - Dept. of Physics
1-130 Knudsen Hall
Los Angeles, CA 90024

Dr. Dennis Gill
Los Alamos National Laboratory
P. O. Box 1663
Los Alamos, NM 87545

Dr. B. B. Godfrey
Mission Research Corporation
1720 Randolph Road, SE
Albuquerque, NM 87106

Dr. P. Goldston
Los Alamos National Laboratory
P. O. Box 1663
Los Alamos, NM 87545

Prof. Louis Hand
Dept. of Physics
Cornell University
Ithaca, NY 14853

Dr. J. Hays
TRW
One Space Park
Redondo Beach, CA 90278

Dr. Wendell Horton
University of Texas
Physics Dept., RLM 11.320
Austin, TX 78712

Dr. J. Y. Hsu
General Atomic
San Diego, CA 92138

Dr. H. Huey
Varian Associates
B-118
611 Hansen Way
Palo Alto, CA 95014

Dr. Robert A. Jameson
Los Alamos National Laboratory
AT-Division, MS H811
P.O. Box 1663
Los Alamos, NM 87545

Dr. G. L. Johnston
NW16-232
M. I. T.
Cambridge, MA 02139

Dr. Shayne Johnston
Physics Department
Jackson State University
Jackson, MS 39217

Dr. Mike Jones
MS B259
Los Alamos National Laboratory
P. O. Box 1663
Los Alamos, NM 87545

Dr. C. Joshi
7620 Boelter Hall
Electrical Engineering Department
University of California, Los Angeles
Los Angeles, CA 90024

Dr. E. L. Kane
Science Applications Intl. Corp.
McLean, VA 22102

Dr. Tom Katsouleas
UCLA, 1-130 Knudsen Hall
Department of Physics
Los Angeles, CA 90024

Dr. Rhon Keinigs MS-259
Los Alamos National Labortory
P. O. Box 1663
Los Alamos, NM 87545

Dr. Kwang-Je Kim
Lawrence Berkeley Laboratory
University of California, Berkeley
Berkeley, CA 94720

Dr. S. H. Kim
Center for Accelerator Technology
University of Texas
P.O. Box 19363
Arlington, TX 76019

Dr. Joe Kindel
Los Alamos National Laboratory
P. O. Box 1663, MS E531
Los Alamos, NM 87545

Dr. Ed Knapp
Los Alamos National Laboratory
P. O. Box 1663
Los Alamos, NM 87545

Dr. Peter Kneisel
Cornell University
F. R. Newman Lab. of Nucl. Studies
Ithaca, NY 14853

Dr. Norman M. Kroll
University of California, San Diego
San Diego, CA 92093

Dr. Kenneth Lee
Los Alamos National Laboratory
P.O. Box 1663, MS E531
Los Alamos, NM 87545

Dr. N. C. Luhmann, Jr.
7702 Boelter Hall
U. C. L. A.
Los Angeles, CA 90024

Dr. K. Maffee
University of Maryland
E. R. B.
College Park, MD 20742

Dr. B. D. McDaniel
Cornell University
Ithaca, NY 14853

Dr. Colin McKinstrie
Los Alamos National Laboratory
P. O. Box 1663
Los Alamos, NM 87545

Dr. A. Mondelli
Science Applications Intl. Corp.
1710 Goodridge Drive
McLean, VA 22101

Dr. Warren Mori
1-130 Knudsen Hall
U. C. L. A.
Los Angeles, CA 90024

Dr. P. L. Morton
Stanford Linear Accelerator Center
P. O. Box 4349
Stanford, CA 94305

Dr. John A. Nation
Laboratory of Plasma Studies
369 Upson Hall
Cornell University
Ithaca, NY 14853

Dr. K. C. Ng
Courant Inst. of Math. Sciences
New York University
New York, NY 10012

Dr. Robert J. Noble
S.L.A.C., Bin 26
Stanford University
P.O. Box 4349
Stanford, CA 94305

Dr. J. Norem
Argonne National Laboratory
Argonne, IL 60439

Dr. Craig L. Olson
Sandia National Laboratories
Plasma Theory Division 1241
P.O. Box 5800
Albuquerque, NM 87185

Dr. H. Oona
MS-E554
Los Alamos National Laboratory
P. O. Box 1663
Los Alamos, NM 87545

Dr. Robert B. Palmer
Brookhaven National Laboratory
Upton, NY 11973

Dr. Richard Pantell
Stanford University
308 McCullough Bldg.
Stanford, CA 94305

Dr. John Pasour
Mission Research Corporation
5503 Cherokee Ave.
Suite 201
Alexandria, VA 22312

Dr. Samual Penner
Center for Radiation Research
National Bureau of Standards
Gaithersburg, MD 20899

Dr. Claudio Pellegrini
National Synchrotron Light Source
Brookhaven National Laboratory
Upton, NY 11973

Dr. Melvin A. Piestrup
Adelphi Technology
13800 Skyline Blvd. No. 2
Woodside, CA 94062

Dr. Z. Pietrzyk
FL-10
University of Washington
Seattle, WA 98185

Dr. Don Prosnitz
Lawrence Livermore National Laboratory
P. O. Box 808
Livermore, CA 94550

Dr. R. Ratowsky
Physics Department
University of California at Berkeley
Berkeley, CA 94720

Dr. Charles W. Roberson
Office of Naval Research
Detachment Arlington
800 North Quincy St., BCT # 1
Arlington, VA 22217-5000

Dr. Stephen Rockwood
Los Alamos National Laboratory
P. O. Box 1663
Los Alamos, NM 87545

Dr. Harvey A. Rose, T-DOT
Los Alamos National Laboratory
Los Alamos, NM 87545

Dr. James B. Rosenzweig
Dept. of Physics
University of Wisconsin
Madison, WI 53706

Dr. Alessandro G. Ruggiero
Argonne National Laboratory
Argonne, IL 60439

Dr. R. D. Ruth
SLAC, Bin 26
P. O. Box 4349
Stanford, CA 94305

Dr. Jack Sandweiss
Gibbs Physics Laboratory
Yale University
260 Whitney Avenue
P. O. Box 6666
New Haven, CT 06511

Dr. Al Saxman
Los Alamos National Laboratory
P.O. Box 1663, MS E523
Los Alamos, NM 87545

Dr. George Schmidt
Stevens Institute of Technology
Department of Physics
Hoboken, NJ 07030

Dr. N. C. Schoen
TRW
One Space Park
Redondo Beach, CA 90278

Dr. Frank Selph
U. S. Department of Energy
Division of High Energy Physics, ER-224
Washington, DC 20545

Dr. Andrew M. Sessler
Lawrence Berkeley Laboratory
University of California, Berkeley
Berkeley, CA 94720

Dr. Richard L. Sheffield
Los Alamos National Laboratory
P.O. Box 1663, MS H825
Los Alamos, NM 87545

Dr. John Siambis
Lockheed Palo Alto Research Laboratory
3251 Hanover Street
Palo Alto, CA 94304

Dr. Robert Siemann
Dept. of Physics
Cornell University
Ithaca, NY 14853

Dr. J. D. Simpson
Argonne National Laboratory
Argonne, IL 60439

Dr. Charles K. Sinclair
Stanford University
P. O. Box 4349
Stanford, CA 94305

Dr. Sidney Singer
MS-E530
Los Alamos National Laboratory
P. O. Box 1663
Los Alamos, NM 87545

Dr. R. Siusher
AT&T Bell Laboratories
Murray Hill, NJ 07974

Dr. Jack Slater
Mathematical Sciences, NW
2755 Northup Way
Bellevue, WA 98009

Dr. Todd Smith
Hansen Laboratory
Stanford University
Stanford, CA 94305

Dr. Richard Spitzer
Stanford Linear Accelerator Center
P. O. Box 4347
Stanford, CA 94305

Mr. J. J. Su
UCLA
1-130 Knudsen Hall
Los Angeles, CA 90024

Prof. Ravi Sudan
Electrical Engineering Department
Cornell University
Ithaca, NY 14853

Dr. Don J. Sullivan
Mission Research Corporation
1720 Randolph Road, SE
Albuquerque, NM 87106

Dr. David F. Sutter
U. S. Department of Energy
Division of High Energy Physics, ER-224
Washington, DC 20545

Dr. T. Tajima
Department of Physics
and Institute for Fusion Studies
University of Texas
Austin, TX 78712

Dr. Lee Teng, Chairman
Fermilab
P.O. Box 500
Batavis, IL 60510

Dr. H. S. Uhm
NSWC
White Oak Laboratory
Silver Spring, MD 20903-5000

U. S. Naval Academy (2 copies)
Director of Research
Annapolis, MD 21402

Dr. William A. Wallenmeyer
U. S. Dept. of Energy
High Energy Physics Div., ER-22
Washington, DC 20545

Dr. John E. Walsh
Department of Physics
Dartmouth College
Hanover, NH 03755

Dr. Tom Wangler
Los Alamos National Laboratory
P. O. Box 1663
Los Alamos, NM 87545

Dr. S. Wilks
Physics Dept.
1-130 Knudsen Hall
UCLA
Los Angles, CA 90024

Dr. Perry B. Wilson
Stanford Linear Accelerator Center
Stanford University
P.O. Box 4349
Stanford, CA 94305

Dr. W. Woo
Applied Science Department
University of California at Davis
Davis, CA 95616

Dr. Jonathan Wurtele
M.I.T.
NW 16-234
Plasma Fusion Center
Cambridge, MA 02139

Dr. Yi-Ton Yan
Los Alamos National Laboratory
MS-K764
Los Alamos, NM 87545

Dr. M. Yates
Los Alamos National Laboratory
P. O. Box 1663
Los Alamos, NM 87545

Dr. Ken Yoshioka
Laboratory for Plasma and Fusion
University of Maryland
College Park, MD 20742

Dr. R. W. Ziolkowski, L-156
Lawrence Livermore National Laboratory
P. O. Box 808
Livermore, CA 94550

END

12-87

DTIC